



Synergistic use of Knudsen effusion quadrupole mass spectrometry, solid-state galvanic cell and differential scanning calorimetry for thermodynamic studies on lithium aluminates

S.K. Rakshit*, Y.P. Naik, S.C. Parida, Smruti Dash, Ziley Singh, B.K. Sen, V. Venugopal

Product Development Section, Radiochemistry and Isotope Group, Bhabha Atomic Research Centre, Trombay, Mumbai 400085, India

ARTICLE INFO

Article history:

Received 31 December 2007

Received in revised form

5 March 2008

Accepted 9 March 2008

Available online 16 March 2008

Keywords:

Breeder material

Lithium aluminate

Knudsen effusion method

Solid-state galvanic cell

Differential scanning calorimetry (DSC)

Heat capacity

Thermodynamic properties

ABSTRACT

Three ternary oxides $\text{LiAl}_5\text{O}_8(\text{s})$, $\text{LiAlO}_2(\text{s})$ and $\text{Li}_5\text{AlO}_4(\text{s})$ in the system Li–Al–O were prepared by solid-state reaction route and characterized by X-ray powder diffraction method. Equilibrium partial pressure of $\text{CO}_2(\text{g})$ over the three-phase mixtures $\{\text{LiAl}_5\text{O}_8(\text{s})+\text{Li}_2\text{CO}_3(\text{s})+5\text{Al}_2\text{O}_3(\text{s})\}$, $\{\text{LiAl}_5\text{O}_8(\text{s})+5\text{LiAlO}_2(\text{s})+2\text{Li}_2\text{CO}_3(\text{s})\}$ and $\{\text{LiAlO}_2(\text{s})+\text{Li}_5\text{AlO}_4(\text{s})+2\text{Li}_2\text{CO}_3(\text{s})\}$ were measured using Knudsen effusion quadrupole mass spectrometry (KEQMS). Solid-state galvanic cell technique based on calcium fluoride electrolyte was used to determine the standard molar Gibbs energies of formations of these aluminates. The standard molar Gibbs energies of formation of these three aluminates calculated from KEQMS and galvanic cell measurements were in good agreement. Heat capacities of individual ternary oxides were measured from 127 to 868 K using differential scanning calorimetry. Thermodynamic tables representing the values of $\Delta_f H^0(298.15 \text{ K})$, $S^0(298.15 \text{ K})$, $S^0(T)$, $C_p^0(T)$, $H^0(T)$, $\{H^0(T)-H^0(298.15 \text{ K})\}$, $G^0(T)$, $\Delta_f H^0(T)$, $\Delta_f G^0(T)$ and free energy function (fef) were constructed using second law analysis and FACTSAGE thermo-chemical database software.

© 2008 Elsevier Inc. All rights reserved.

1. Introduction

Lithium–aluminum–oxygen system has four ternary oxides: $\text{LiAl}_5\text{O}_8(\text{s})$, $\text{LiAlO}_2(\text{s})$, $\text{Li}_3\text{AlO}_3(\text{s})$ and $\text{Li}_5\text{AlO}_4(\text{s})$; however, $\text{Li}_3\text{AlO}_3(\text{s})$ is reported to be unstable above 670 K [1,2]. Among these oxides, $\text{LiAlO}_2(\text{s})$ has gained importance for its potential use as breeder material in the irradiation blanket for future nuclear fusion reactors due to its chemical and thermal stability as well as less radiation damage [3]. This oxide exists in three possible allotropes, hexagonal α - LiAlO_2 up to 673 K, monoclinic β - LiAlO_2 from 673 to 1073 K and tetragonal γ - LiAlO_2 , the most stable form at temperature greater than 1073 K. This aluminate is also used as an inert and non-conductive ceramic matrix to contain molten carbonate electrolyte between the anode and the cathode of molten carbonate fuel cells due to its high mechanical and thermal stability [3–5]. This aluminate is also expected to be less reactive with cladding materials presently used in fusion reactors due to lower vapor pressures and higher melting points than solid Li_2O . Many researchers have carried out the preparation, decomposition and thermal studies of $\text{LiAlO}_2(\text{s})$ [6,7] but studies on other aluminates in Li–Al–O system are very scarce. Ikeda et al. [1]

have studied the vaporization and thermo-chemical stability of lithium aluminates using high-temperature Knudsen effusion mass spectrometry. Many researchers have reported the enthalpy and heat capacity values of LiAlO_2 from 298 to 1700 K [8]. Kleykamp [8] has reported the heat capacity of $\text{LiAlO}_2(\text{s})$. In this study, thermodynamic properties of $\text{LiAl}_5\text{O}_8(\text{s})$, $\text{LiAlO}_2(\text{s})$ and $\text{Li}_5\text{AlO}_4(\text{s})$ were determined using Knudsen effusion quadrupole mass spectrometry (KEQMS), solid-state galvanic cell based on CaF_2 solid electrolyte and differential scanning calorimetry (DSC).

2. Experimental

2.1. Materials preparation

Ternary oxides, $\text{LiAl}_5\text{O}_8(\text{s})$, $\text{LiAlO}_2(\text{s})$ and $\text{Li}_5\text{AlO}_4(\text{s})$, were prepared using conventional solid-state reaction route using pre-heated powder samples of $\text{Li}_2\text{CO}_3(\text{s})$ and $\text{Al}_2\text{O}_3(\text{s})$ (LEICO Industries Inc., mass fraction 0.9999). The individual powders were weighed according to their stoichiometric ratios and mixed homogeneously using an agate mortar and pestle and the resultant powder samples were pelletized using a steel die at a pressure of 100 MPa. The pellets were initially heated at 900 K for 50 h in air in a re-crystallized alumina crucible and then cooled, reground and again pelletized. These pellets were then heated at

* Corresponding author. Fax: +91 22 2550 5151.

E-mail addresses: swarupkr@barc.gov.in, swarup_kr@rediffmail.com (S.K. Rakshit).

1150 K for 48 h. The resultant samples were characterized by X-ray powder diffraction (XRD) technique using DIANO XRD with Cu-K α radiation and graphite monochromator and found to be pure crystalline phases of LiAl₅O₈(s), γ -LiAlO₂(s) and β -Li₅AlO₄(s).

Three-phase mixtures {LiAl₅O₈(s)+Li₂CO₃(s)+5Al₂O₃(s)}, {LiAl₅O₈(s)+2Li₂CO₃(s)+5LiAlO₂(s)} and {LiAlO₂(s)+2Li₂CO₃(s)+Li₅AlO₄(s)} for KEQMS were prepared by homogeneously mixing the individual pre-heated compounds in stoichiometric ratios and pelletized using a steel die and then sintered at 700 K to remove moisture. The sintered pellets were broken into small pieces and loaded inside the Knudsen cell.

According to the phase relations in the Li₂O–Al₂O₃ pseudo-binary system, phase mixtures: {2LiAl₅O₄(s)+5Al₂O₃(s)+2LiF(s)}, {5LiAlO₂(s)+LiAl₅O₄(s)+4LiF(s)} and {Li₅AlO₄(s)+LiAlO₂(s)+4LiF(s)} were also prepared by homogeneously mixing the pre-heated individual powders and pelletized using a steel die at a pressure of 100 MPa and sintered at 800 K for 10 h under moisture and hydrogen-free oxygen atmosphere. These sample pellets were then used for solid-state galvanic cell experiments. Powder samples of LiAl₅O₈(s), LiAlO₂(s) and Li₅AlO₄(s) were used for DSC.

2.2. Knudsen effusion quadrupole mass spectrometry (KEQMS)

The Knudsen effusion mass spectrometric technique is one of the most informative methods for vaporization processes and thermodynamic properties of high-temperature systems. Generally, for thermodynamic measurements, traditional magnetic sector mass spectrometer attached to Knudsen effusion system is preferable among quadrupole and time-of-flight mass spectrometers. Murray et al. [9] have shown that thermodynamic data obtained by Knudsen effusion technique using magnetic sector spectrometer and quadrupole mass spectrometer are in good agreement for pure chromium and chromium–silicon samples. However, quadrupole mass spectrometer has no significant advantages over magnetic mass spectrometer but they are very compact and relatively inexpensive. Stolyarova et al. [10] have reported that quadrupole mass spectrometer coupled to Knudsen cell can effectively be used for thermodynamic studies at high temperature.

In this study, a residual gas analyzer (RGA) coupled to Knudsen effusion system was used for equilibrium partial pressure measurements. An RGA is a quadrupole mass spectrometer in which the ionizer is immersed in the gas to be analyzed, and the ionizer is characterized by an open construction in which the gas may enter and leave in all directions. It is assumed that the gas is homogenous and that changes in the gas density with time occur slowly enough such that the instrument is always in equilibrium with the gas. This instrument can be used to identify the kind of molecules present in the gaseous phase and, when calibrated, can be used to determine concentrations or partial pressures [11–13] of individual species.

The KEQMS used in this study is an in-house designed Knudsen vacuum chamber and arranged in such a way that it allows reciprocally perpendicular molecular beam from the Knudsen effusion cell. The Knudsen vacuum chamber was heated to the desired temperature using resistance heater. The temperature near the Knudsen cell was measured using a pre-calibrated (ITS-90) chromel–alumel thermocouple. The Knudsen cell used was made of 15 mol% calcia stabilized zirconia (CSZ) with a thin cylindrical orifice of dia 0.8 mm and height 0.2 mm at the centre of the lid. This setup is used only for partial pressures measurements of permanent gaseous species such as CO, O₂, N₂, CO₂, etc. and not for condensable vapor species. A shutter is placed between the ionizer and the Knudsen effusion chamber such that it does not

come into the path of the molecular flow. The shutter isolates the Knudsen effusion cell while recording the background signal.

The detected signal (I_i^+) measured using Faraday cup detector is related to the partial pressure of the vapor species (p_i) by

$$p_i = K_{\text{inst}} I_i^+ T / (\sigma_i a_i) \quad (1)$$

where K_{inst} is the instrumental constant, I_i^+ is the measured ion current in ampere, T is the absolute temperature near the Knudsen cell, σ_i is the electron impact cross-section and a_i isotopic abundance of the specific ion. Eq. (1) can be represented as

$$\ln p_i = \ln K_{\text{inst}} + \ln(I_i^+ T) - \ln \sigma_i - \ln a_i \quad (2)$$

For permanent gaseous species such as CO₂ at mass, $m = 44$, $\ln \sigma = -45.52$ at 30 eV [14] and the isotopic abundance as 100%, Eq. (2) can be expressed as

$$\ln P_i = \ln K_{\text{inst}} + \ln(I_i^+ T) + 45.52 \quad (\text{for } i = \text{CO}_2) \quad (3)$$

2.2.1. Calibration of KEQMS

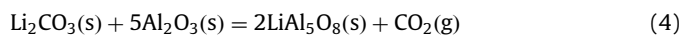
Prior to calibration of the instrument, the background signals were monitored by heating the Knudsen chamber with empty Knudsen cell at different temperatures from ambient to 1161 K at pressure level $\sim 1 \times 10^{-5}$ Pa. The background signals as a function of temperature are shown in Fig. 1. It is evident from the figure that the background signals corresponding to H₂⁺, N₂⁺, CO⁺ and CO₂⁺ do not change appreciably with change in temperature. During experiments, the actual signals were obtained by subtracting the ion intensities due to background.

The instrument calibration constant (K_{inst}) was determined by measuring the ion intensities of CO₂⁺ over the phase mixtures of {CaCO₃(s)+CaO(s)}, {SrCO₃(s)+SrO(s)}, {BaCO₃(s)+BaO(s)} and {Li₂CO₃(s)+Li₂O(s)}. Three different ionization energies (30, 50 and 70 eV) were used to measure the ion intensities of CO₂⁺ to check the linearity of pressure measurements. However, 30 eV is sufficient to ionize all types of gaseous molecules; hence, the actual experiments were carried out at ionization energy of 30 eV. Prior to actual measurement, a particular phase mixture (mass ~ 1 g) was loaded inside the Knudsen cell and then heated at 700 K for 4 h under high vacuum to remove the moisture and other unwanted gaseous species.

2.2.2. Partial pressure measurements of CO₂(g) over equilibrium phase mixtures

Huang et al. [15] have reported the thermodynamic data of Na₄Fe₆O₁₁(s) by measuring the partial pressure of CO₂(g) over {2Na₂CO₃(s)+3Fe₂O₃(s)} phase mixture using Knudsen effusion mass spectrometry from 918 to 1013 K. Similar approach was adopted in this study to determine the Gibbs energies of formation of LiAl₅O₈(s), LiAlO₂(s) and Li₅AlO₄(s) by measuring the partial pressure of CO₂(g) over the equilibrium phase mixtures {LiAl₅O₈(s)+Li₂CO₃(s)+5Al₂O₃(s)}, {LiAl₅O₈(s)+2Li₂CO₃(s)+5LiAlO₂(s)} and {LiAlO₂(s)+2Li₂CO₃(s)+Li₅AlO₄(s)}.

The ion intensities of CO₂⁺ over these equilibrium phase mixtures were measured using KEQMS. For each measurement, two sets of experiments were carried out and the ion intensities for other gaseous species were in background level during the measurement. Subsequently, partial pressures of carbon dioxide, $p(\text{CO}_2)$ over the phase mixture were obtained using Eq. (3). After the mass spectrometric measurements, the resultant phase mixtures were analyzed by XRD technique and found to be the mixture of corresponding lithium aluminate, lithium carbonate and alumina. Therefore, it was assumed that the following equilibrium reactions were established inside the Knudsen cell under experimental conditions:



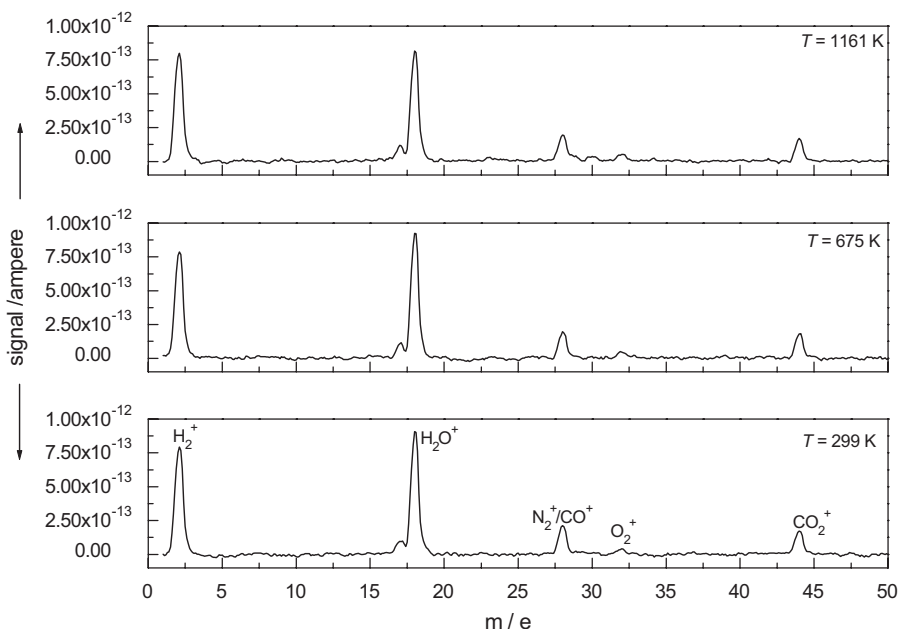
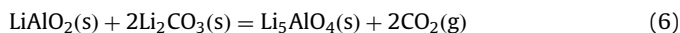
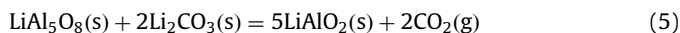


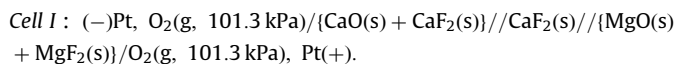
Fig. 1. Background spectrum of the mass spectrometer with blank Knudsen cell as a function of temperature.



Therefore, the measured $p(\text{CO}_2)$ corresponds to the equilibrium partial pressures of the above reactions.

2.3. Solid-state galvanic cell technique with CaF_2 electrolyte

The experimental setup and the cell assembly used in this study have been explained in details by Rakshit et al. [16]. A schematic diagram of the fluoride cell used in this experiment is shown in Fig. 2. Optical grade single crystal of $\text{CaF}_2(\text{s})$ pellet of 6 mm diameter and 3 mm thickness (supplied by Solon Technologies, Inc., USA) was used as fluoride ion conducting electrolyte. It is a single compartment cell with provisions for passing purified oxygen gas during the experiment and to measure the temperature of the cell near the electrode/electrolyte interface. High-purity oxygen gas at one atmospheric pressure was allowed to pass through successive traps of silica gels, molecular sieves, oxidized form of BTS catalyst and anhydrous magnesium perchlorate for removal of traces of $\text{H}_2(\text{g})$ and moisture. The reference electrode, the electrolyte and the sample electrode stacked one over the other was kept in the isothermal temperature zone of a Kanthal wire wound furnace. The furnace temperature was controlled within ± 1 K using a PID temperature controller. The cell was standardized using phase mixtures of $\{\text{CaO}(\text{s})+\text{CaF}_2(\text{s})\}$ and $\{\text{MgO}(\text{s})+\text{MgF}_2(\text{s})\}$ as two standard electrodes. The cell can be represented as



After standardization, the reversible emf's of the following solid-state galvanic cells were measured as a function of temperature.

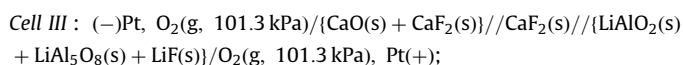
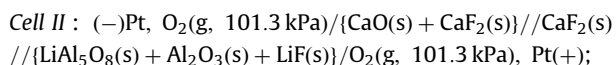
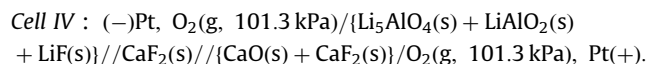


Fig. 2. Schematic diagram of the fluoride cell. (1) Pt lead wires, (2) alumina pressing tube, (3) thermocouple, (4) stainless-steel flange, (5) gas inlet, (6) gas outlet, (7) spring, (8) quartz tube; (9) quartz tube, (10) alumina cup, (11) Pt discs, (12) kanthal wire wound furnace, (13) reference electrode, (14) $\text{CaF}_2(\text{s})$ electrolyte and (15) sample electrode.



The cell temperature close to the electrodes was measured using a pre-calibrated (ITS-90) chromel–alumel thermocouple. The cell emf (± 0.02 mV) was measured by using a Keithley 614

electrometer (input impedance $>10^{14}\Omega$). At low temperatures, stable values of emf were obtained approximately after 72 h whereas at successive higher temperatures, stability in emf values was observed within 5–6 h. The reversibility of the solid-state electrochemical cells was evaluated by micro-coulometric titration in both directions. The electrode pellets after the emf measurements were re-examined by XRD analysis and the phase compositions were found unchanged.

2.4. Measurement of heat capacity using differential scanning calorimetry

Molar heat capacity measurements were carried out using a heat flux-type DSC (131, Setaram Instrumentation, France). The temperature and energy calibrations and the methods of heat capacity measurements by continuous heating mode were described in details by Rakshit et al. [16]. In order to check the accuracy of the measurement, heat capacity of Fe_2O_3 (mass fraction 0.9999, Alfa Aesar, USA) was measured in the temperature range from (i) 130 to 320 and (ii) 310–860 K. The values of heat capacity of $\text{Fe}_2\text{O}_3(\text{s})$ were found to be within $\pm 2\%$ compared to the literature values [17]. The pre-heated powder samples of $\text{LiAl}_5\text{O}_8(\text{s})$, $\text{LiAlO}_2(\text{s})$ and $\text{Li}_5\text{AlO}_4(\text{s})$ were used for heat capacity measurements.

3. Results and discussion

3.1. KEQMS technique

3.1.1. Calibration of KEQMS (K_{inst})

The ion intensities of CO_2^+ over the phase mixtures $\{\text{CaCO}_3(\text{s})+\text{CaO}(\text{s})\}$, $\{\text{SrCO}_3(\text{s})+\text{SrO}(\text{s})\}$, $\{\text{BaCO}_3(\text{s})+\text{BaO}(\text{s})\}$ and $\{\text{Li}_2\text{CO}_3(\text{s})+\text{Li}_2\text{O}(\text{s})\}$ were recorded in ampere using Faraday cup detector as a function of temperature for two different runs. The values of $\ln(K_{\text{inst}})$ were calculated as a function of temperature using Eq. (3), literature values of $\ln\{p(\text{CO}_2)/\text{Pa}\}$ [17] and experimentally measured $\ln(I_i^+T)$ values and represented in Table 1. The calibration constant calculated at 30 eV for $\{\text{Li}_2\text{CO}_3(\text{s})+\text{Li}_2\text{O}(\text{s})\}$ phase mixture was used for further calculation and is expressed as

$$\ln(K_{\text{inst}}) = 3711.9/(T(\text{K})) - 47.05 \quad (614 \leq T(\text{K}) \leq 750) \quad (7)$$

An ideal instrument has a sensitivity that is constant and independent of pressure. The ion current reaching the detector of such an instrument should, therefore, increase linearly with

pressure. The sensitivity of the experimental system was checked by plotting the detected signals (ampere) as a function of literature values of partial pressure of $\text{CO}_2(\text{g})$ over the respective carbonate-oxide phase fields and shown in Fig. 3. This figure shows that the detected ion currents varies linearly as a function of partial pressure of $\text{CO}_2(\text{g})$ throughout the measurement range.

3.1.2. Equilibrium partial pressures over the ternary phase mixtures

3.1.2.1. The phase mixture $\{\text{LiAl}_5\text{O}_8(\text{s})+\text{Li}_2\text{CO}_3(\text{s})+5\text{Al}_2\text{O}_3(\text{s})\}$. The ion intensities of CO_2^+ peak over $\{\text{LiAl}_5\text{O}_8(\text{s})+\text{Li}_2\text{CO}_3(\text{s})+5\text{Al}_2\text{O}_3(\text{s})\}$ phase mixture was measured at 30 eV ionization energy in the temperature range 614–750 K. Partial pressures of $\text{CO}_2(\text{g})$, $p(\text{CO}_2)$, at different temperatures for two different runs were calculated using the measured ion intensities, Eq. (3) and the calibration constant from Eq. (7) and the values are listed in Table 2. The variation of logarithmic values of $p(\text{CO}_2)$ as a function of reciprocal of temperature follows linear relationship as shown in Fig. 4 and can be expressed as

$$\ln\{p(\text{CO}_2(\text{Pa}))\} = -18412.1(\pm 260.2)/(T(\text{K})) + 24.44(\pm 0.38) \quad (8)$$

The enthalpy change associated with reaction (4) at the average temperature of the measurement was estimated to be $\Delta_{\text{r}(4)}H_{\text{m}}^0(682\text{K}) = (153.1 \pm 2.2)\text{kJ mol}^{-1}$. The standard molar Gibbs energy of formation ($\Delta_{\text{f}}G_{\text{m}}^0$) of $\text{LiAl}_5\text{O}_8(\text{s})$ from the elements was calculated from Eqs. (4) and (8) and the values of $\Delta_{\text{f}}G_{\text{m}}^0(T)$ for $\text{Li}_2\text{CO}_3(\text{s})$, $\text{Al}_2\text{O}_3(\text{s})$ and $\text{CO}_2(\text{g})$ from the literature [17] and can be represented as

$$\Delta_{\text{f}}G_{\text{m}}^0(\text{LiAl}_5\text{O}_8, \text{s}, T)\text{kJ mol}^{-1} = -4522.2 + 0.8725(T(\text{K})) \pm 2.4 \quad (614 \leq T(\text{K}) \leq 750) \quad (9)$$

3.1.2.2. The phase mixture $\{\text{LiAl}_5\text{O}_8(\text{s})+2\text{Li}_2\text{CO}_3(\text{s})+5\text{LiAlO}_2(\text{s})\}$. The ion intensities of CO_2^+ peak over the phase mixture $\{\text{LiAl}_5\text{O}_8(\text{s})+2\text{Li}_2\text{CO}_3(\text{s})+5\text{LiAlO}_2(\text{s})\}$ was measured at 30 eV ionization energy in the temperature range 604–723 K. Partial pressures of $\text{CO}_2(\text{g})$, $p(\text{CO}_2)$, at different temperatures for two different runs were calculated using the measured ion intensities, Eq. (5) and the calibration constant from Eq. (7) and the values are listed in Table 2. The variation of logarithmic values of $p(\text{CO}_2)$ as a function of reciprocal of temperature follows linear relationship as shown in Fig. 4 and can be expressed as

$$\ln\{p(\text{CO}_2(\text{Pa}))\} = -18064.8(\pm 365.5)/(T(\text{K})) + 25.27(\pm 0.55) \quad (10)$$

Table 1
Ion intensities of CO_2^+ at different ion energies over different phase mixtures

Phase	Ionization energy (eV)	Combined $\ln(I_i^+T)$ of two runs	$\ln(P_i/\text{atm})$ literature [15]	Temperature range (K)
$\text{CaCO}_3(\text{s})+\text{CaO}(\text{s})$	30	$-25191.1/T+18.44$	$-21093.3/T+18.53$	604–772
	50	$-26090.3/T+21.10$		617–764
	70	$-25452.4/T+20.28$		622–781
$\text{SrCO}_3(\text{s})+\text{SrO}(\text{s})$	30	$-28649.7/T+16.16$	$-28792.7/T+19.85$	832–951
	50	$-30706.4/T+19.48$		833–978
	70	$-29566.4/T+19.37$		835–939
$\text{BaCO}_3(\text{s})+\text{BaO}(\text{s})$	30	$-33203.1/T+17.64$	$-31664.9/T+19.57$	821–1055
	50	$-32296.9/T+18.28$		822–1056
	70	$-32531.8/T+19.17$		838–1043
$\text{Li}_2\text{CO}_3(\text{s})+\text{Li}_2\text{O}(\text{s})$	30	$-29594.2/T+19.17$	$-25882.3/T+17.64$	688–887
	50	$-26523.2/T+16.78$		676–885
	70	$-26677.2/T+17.40$		686–889

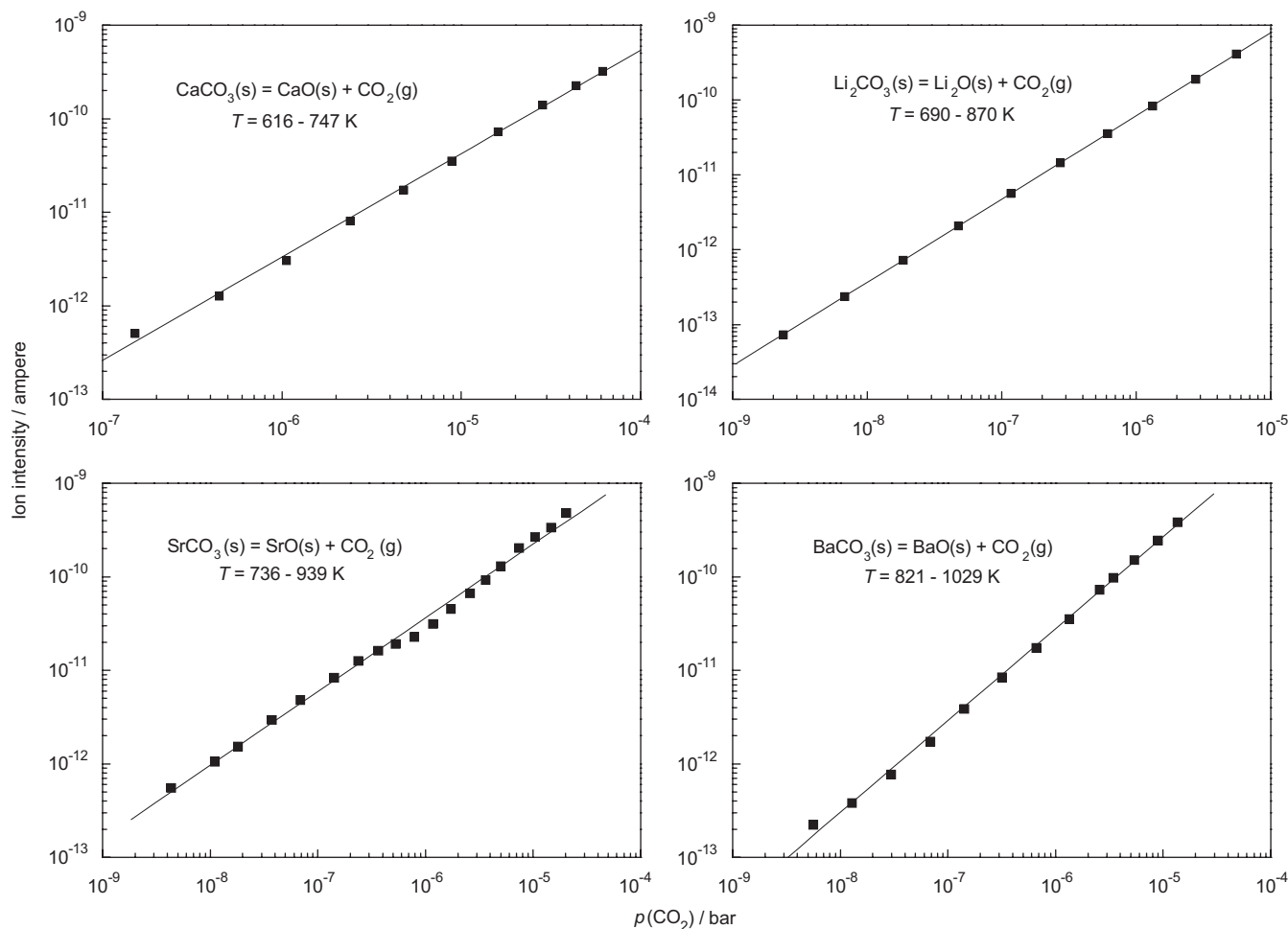


Fig. 3. Ion intensities of CO_2^+ peak over various carbonate–oxide phase mixtures as a function of literature values of $p(\text{CO}_2)$.

The enthalpy change associated with reaction (5) at the average temperature of the measurement was estimated to be $\Delta_{r(5)}H_m^0(664\text{ K}) = (150.2 \pm 3.0)\text{ kJ mol}^{-1}$. The standard molar Gibbs energy of formation ($\Delta_f G_m^0$) of $\text{LiAlO}_2(\text{s})$ from the elements was calculated from Eqs. (5) and (10) and the values of $\Delta_f G_m^0(T)$ for $\text{Li}_2\text{CO}_3(\text{s})$, $\text{Al}_2\text{O}_3(\text{s})$ and $\text{CO}_2(\text{g})$ from the literature [17] and $\Delta_f G_m^0(\text{LiAl}_5\text{O}_8, \text{s}, T)$ from Eq. (9) and can be represented as

$$\Delta_f G_m^0(\text{LiAlO}_2, \text{s}, T)\text{ kJ mol}^{-1} = -1171.9 + 0.2423(T\text{ (K)}) \quad (\pm 4.0) (604 \leq T\text{ (K)} \leq 723) \quad (11)$$

3.1.2.3. The phase mixture $\{\text{LiAlO}_2(\text{s}) + 2\text{Li}_2\text{CO}_3(\text{s}) + \text{Li}_5\text{AlO}_4(\text{s})\}$. The ion intensities of CO_2^+ peak over $\{\text{LiAlO}_2(\text{s}) + 2\text{Li}_2\text{CO}_3(\text{s}) + \text{Li}_5\text{AlO}_4(\text{s})\}$ phase mixture was measured at 30 eV ionization energy in the temperature range 614–750 K. Partial pressures of $\text{CO}_2(\text{g})$, $p(\text{CO}_2)$, at different temperatures for two different runs were calculated using the measured ion intensities, Eq. (6) and the calibration constant from Eq. (7) and the values are listed in Table 2. The variation of logarithmic values of $p(\text{CO}_2)$ as a function of reciprocal of temperature follows linear relationship as shown in Fig. 4 and can be expressed as

$$\ln\{p(\text{CO}_2\text{ (Pa)})\} = -28166.5(\pm 544.7)/(T\text{ (K)}) + 34.97(\pm 0.74) \quad (12)$$

The enthalpy change associated with reaction (6) at the average temperature of the measurement was estimated to be $\Delta_{r(6)}H_m^0(739\text{ K}) = (234.2 \pm 4.5)\text{ kJ mol}^{-1}$. The standard molar Gibbs

energy of formation ($\Delta_f G_m^0$) of $\text{Li}_5\text{AlO}_4(\text{s})$ from the elements was calculated from Eqs. (6) and (12) and the values of $\Delta_f G_m^0(T)$ for $\text{Li}_2\text{CO}_3(\text{s})$, $\text{Al}_2\text{O}_3(\text{s})$ and $\text{CO}_2(\text{g})$ from the literature [17] and $\Delta_f G_m^0(\text{LiAlO}_2, \text{s}, T)$ from Eq. (11) and can be represented as

$$\Delta_f G_m^0(\text{Li}_5\text{AlO}_4, \text{s}, T)\text{ kJ mol}^{-1} = -2341.3 + 0.4201(T\text{ (K)}) \quad (\pm 5.5) (672 \leq T\text{ (K)} \leq 806) \quad (13)$$

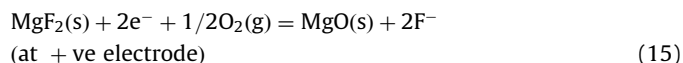
3.2. Emf studies on cells (I)–(IV) using solid-state galvanic cell technique

3.2.1. Standardization of solid-state galvanic cell (I)

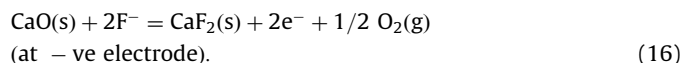
The reversible emf values obtained at different experimental temperatures for cell (I) are listed in Table 3 and the variation of emf with temperature is shown in Fig. 5. The emf data were least-squares fitted to yield the following linear relation:

$$E\text{ (V)}(\pm 0.0002) = 0.3956 - 2.1073 \times 10^{-5}(T\text{ (K)}) \quad (921 \leq T\text{ (K)} \leq 1150) \quad (14)$$

The half-cell reactions at each electrode can be represented as



and



The net virtual cell reaction can be represented as



The Gibbs free energy change for the net cell reaction is calculated from the general relation:

$$\Delta_r G^0 = -nFE \quad (18)$$

Table 2

Partial pressures of $\text{CO}_2(\text{g})$ over $\{\text{LiAl}_5\text{O}_8 + \text{Li}_2\text{CO}_3 + 5\text{Al}_2\text{O}_3\}$, $\{\text{LiAl}_5\text{O}_8 + 5\text{LiAlO}_2 + 2\text{Li}_2\text{CO}_3\}$ and $\{\text{LiAlO}_2 + \text{Li}_5\text{AlO}_4 + 2\text{Li}_2\text{CO}_3\}$ determined from KEQMS as a function of temperature

Reaction (4)		Reaction (5)		Reaction (6)	
T (K)	$p(\text{CO}_2)$ (Pa)	T (K)	$p(\text{CO}_2)$ (Pa)	T (K)	$p(\text{CO}_2)$ (Pa)
Run 1					
625	0.00614	610	0.01612	680	0.00128
639	0.01224	623	0.02957	690	0.00234
655	0.02622	634	0.04840	700	0.00420
665	0.03991	644	0.07466	710	0.00741
678	0.06389	655	0.11849	720	0.01287
688	0.09048	671	0.22572	730	0.02202
698	0.13369	685	0.38709	740	0.03713
709	0.20509	701	0.69819	750	0.06173
718	0.27984	713	1.06802	760	0.10127
730	0.40107	723	1.50569	770	0.16401
738	0.52235	733	2.10282	780	0.26237
750	0.77532	750	3.63553	790	0.41474
				800	0.64813
Run 2					
614	0.00441	604	0.00874	672	0.00118
629	0.00747	616	0.01548	684	0.00245
649	0.01987	626	0.02451	696	0.00498
665	0.03991	636	0.03825	706	0.00883
676	0.06510	642	0.04963	716	0.01540
688	0.09513	652	0.07579	726	0.02645
699	0.15801	662	0.11426	736	0.04476
709	0.24541	669	0.15118	746	0.07470
720	0.37522	679	0.22331	756	0.12298
732	0.58085	692	0.36459	766	0.19985
743	0.89149	697	0.43811	776	0.32073
		706	0.60579	786	0.50856
		719	0.96763	796	0.79710
				806	1.23550

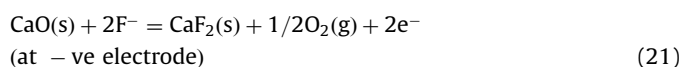
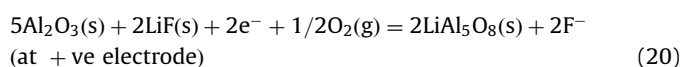
where 'n' is the total number of electrons involved in the half-cell reactions and 'F' is the Faraday's constant ($F = 96486.4 \text{ C mol}^{-1}$) and 'E' is the net cell emf in volts. The values of $\Delta_{r(17)}G^0(T)$ as a function of temperature can be calculated using Eqs. (14) and (18) ($n = 2$) and is represented by the following expression:

$$\Delta_{r(17)}G^0(T) \text{ kJ mol}^{-1} (\pm 0.1) = -76.3 + 0.0041 (T \text{ (K)}) \quad (921 \leq T \text{ (K)} \leq 1150) \quad (19)$$

The values of $\Delta_{r(17)}G^0(T)$ obtained in this study are in good agreement ($\pm 2.0 \text{ kJ mol}^{-1}$) with those calculated using the values of standard molar Gibbs free energy of formations for $\text{CaF}_2(\text{s})$, $\text{MgF}_2(\text{s})$, $\text{MgO}(\text{s})$ and $\text{CaO}(\text{s})$ from the literature [17].

3.2.2. $\Delta_f G^0(T)$ for $\text{LiAl}_5\text{O}_8(\text{s})$

The reversible emf values obtained at different temperatures from 785 to 1036 K for cell (II) are listed in Table 3 and the variation of emf with temperature is shown in Fig. 5. The half-cell reactions at each electrode can be represented as



Hence, the net cell reaction can be written as



The emf data were least-squares fitted to yield the following linear relation:

$$\text{Cell (II)} : E \text{ (V)} (\pm 0.0020) = 0.1820 - 1.5799 \times 10^{-4} (T \text{ (K)}). \quad (785 \leq T \text{ (K)} \leq 1036) \quad (23)$$

The Gibbs free energy change for the equilibrium reaction (22) can be calculated using Eqs. (18) ($n = 2$) and (23) and is represented as

$$\Delta_{r(22)}G^0(T) \text{ kJ mol}^{-1} (\pm 0.02) = -35.1 + 0.0305 (T \text{ (K)}) \quad (785 \leq T \text{ (K)} \leq 1036) \quad (24)$$

The standard molar Gibbs energy of formation $\Delta_f G_m^0(\text{LiAl}_5\text{O}_8, \text{s}, T)$ was obtained by using Eqs. (22) and (24) and values of $\Delta_f G_m^0(T)$

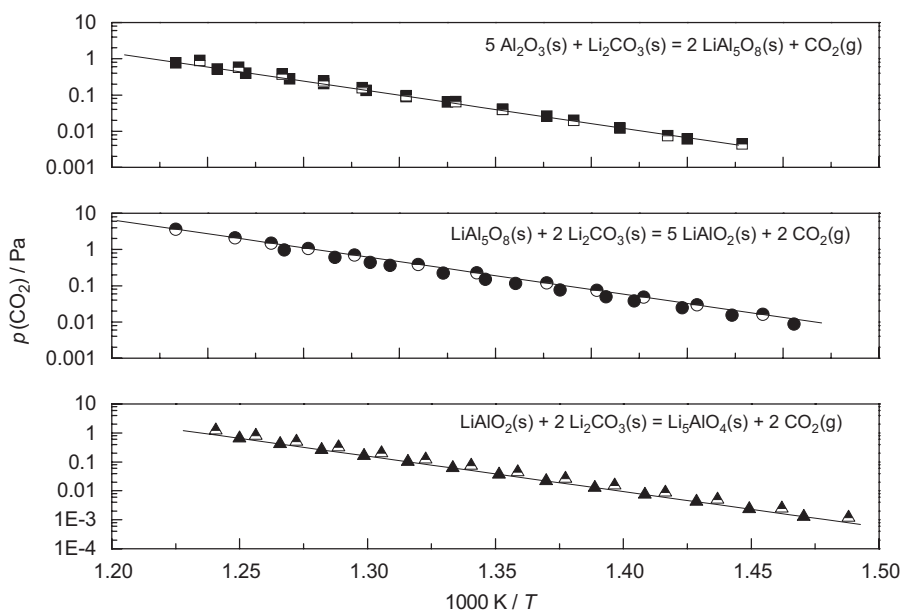


Fig. 4. Partial pressure of $\text{CO}_2(\text{g})$ for reactions (4)–(6) as a function of temperature for two experimental runs with same phase mixtures.

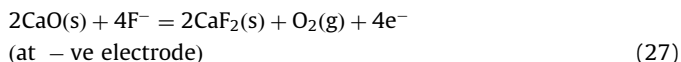
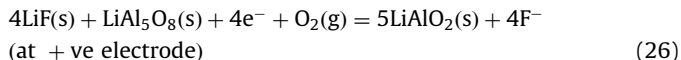
for $\text{Al}_2\text{O}_3(\text{s})$, $\text{CaO}(\text{s})$, $\text{LiF}(\text{s})$ and $\text{CaF}_2(\text{s})$ from literature [17] and represented as

$$\Delta_f G_m^0(T) \text{ kJ mol}^{-1} (\pm 2.9) = -4545.0 + 0.8818 (T \text{ (K)}) \quad (785 \leq T \text{ (K)} \leq 1036). \quad (25)$$

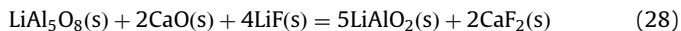
3.2.3. $\Delta_f G^0(T)$ for $\text{LiAlO}_2(\text{s})$

The reversible emf values obtained at different experimental temperatures for cell (III) are listed in Table 3 and the variation of

emf with temperature is shown in Fig. 5. The half-cell reactions at each electrode can be represented as



Hence, the net cell reaction can be written as



The emf data were least-squares fitted to yield the following linear relation:

$$\text{Cell (III)} : E \text{ (V)} (\pm 0.0020) = -0.1569 + 2.3522 \times 10^{-4} (T \text{ (K)}), \quad (719 \leq T \text{ (K)} \leq 929) \quad (29)$$

The Gibbs free energy change for the equilibrium reaction (28) can be calculated using Eqs. (18) ($n=4$) and (29) and is represented as

$$\Delta_{r(28)} G^0(T) \text{ kJ mol}^{-1} (\pm 0.7) = 60.6 - 0.0908 (T \text{ (K)}) \quad (719 \leq T \text{ (K)} \leq 929). \quad (30)$$

The standard molar Gibbs energy of formation $\Delta_f G_m^0$ (LiAlO_2 , s, T) was obtained by using Eqs. (28) and (30) and values of $\Delta_f G_m^0(T)$ for $\text{LiAl}_5\text{O}_8(\text{s})$ from Eq. (25), $\text{CaO}(\text{s})$, $\text{LiF}(\text{s})$ and $\text{CaF}_2(\text{s})$ from literature [17] and represented as

$$\Delta_f G_m^0(T) \text{ kJ mol}^{-1} (\pm 4.5) = -1157.8 + 0.2118 (T \text{ (K)}) \quad (719 \leq T \text{ (K)} \leq 929). \quad (31)$$

3.2.4. $\Delta_f G^0(T)$ for $\text{Li}_5\text{AlO}_4(\text{s})$

The reversible emf values obtained at different experimental temperatures for cell (IV) are listed in Table 3 and the variation of

Table 3
Variation of emf as a function of temperature for cells (I)–(IV)

Cell (I)		Cell (II)		Cell (III)		Cell (IV)	
T (K)	E (V)	T (K)	E (V)	T (K)	E (V)	T (K)	E (V)
921	0.3762	785	0.0591	719	0.0107	734	0.2077
941	0.3758	793	0.0565	734	0.0157	747	0.2068
960	0.3754	803	0.0544	748	0.0169	756	0.2043
982	0.3749	813	0.0529	760	0.0217	769	0.2038
1000	0.3746	826	0.0535	771	0.0244	777	0.2011
1019	0.3741	833	0.0496	780	0.0260	789	0.2000
1042	0.3736	842	0.0494	790	0.0289	795	0.1991
1060	0.3733	854	0.0465	801	0.0329	807	0.1974
1072	0.3730	864	0.0458	811	0.0338	819	0.1953
1088	0.3727	873	0.0437	819	0.0365	832	0.1935
1101	0.3724	885	0.0395	829	0.0381	843	0.1927
1122	0.3720	894	0.0407	837	0.0437		
1134	0.3717	905	0.0369	850	0.0430		
1150	0.3714	913	0.0382	866	0.0469		
		923	0.0349	871	0.0504		
		933	0.0362	882	0.0505		
		942	0.0330	890	0.0534		
		956	0.0330	900	0.0548		
		961	0.0300	908	0.0553		
		971	0.0328	920	0.0576		
		984	0.0265	929	0.0591		
		993	0.0300				
		1000	0.0200				
		1009	0.0266				
		1015	0.0191				
		1036	0.0141				

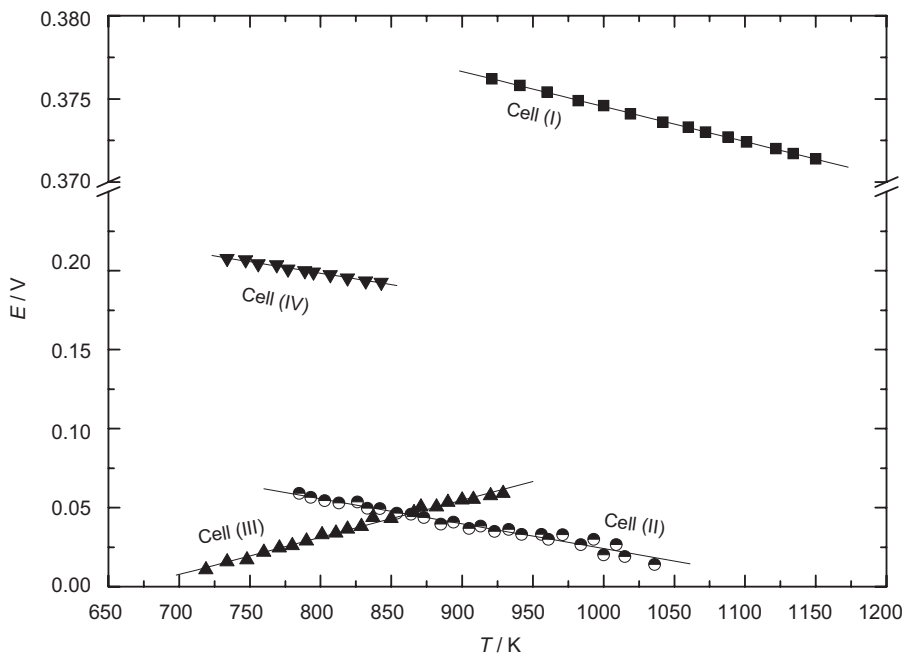
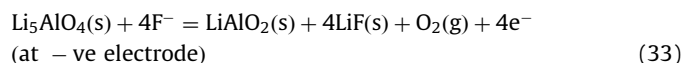
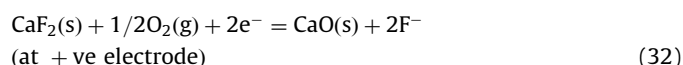
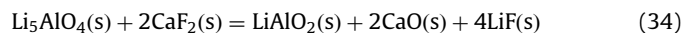


Fig. 5. Emf values of cells (I)–(IV) as a function of temperature.

emf with temperature is shown in Fig. 5. The half-cell reactions at each electrode can be represented as



Hence, the net cell reaction can be written as



The emf data were least-squares fitted to yield the following linear relation:

$$\text{Cell (IV)} : E (\text{V}) (\pm 0.0006) = 0.3145 - 1.4517 \times 10^{-4} (T (\text{K})), \quad (734 \leq T (\text{K}) \leq 843) \quad (35)$$

The Gibbs free energy change for the equilibrium reaction (34) can be calculated using Eqs. (18) ($n = 4$) and (35) and is represented as

$$\Delta_{\text{r}(34)} G^0(T) \text{ kJ mol}^{-1} (\pm 0.2) = -121.4 + 0.0560 (T (\text{K})), \quad (734 \leq T (\text{K}) \leq 843). \quad (36)$$

The standard molar Gibbs energy of formation $\Delta_{\text{f}} G_{\text{m}}^0(\text{Li}_5\text{AlO}_4, \text{s}, T)$ was obtained by using Eqs. (34) and (36) and values of $\Delta_{\text{f}} G_{\text{m}}^0(T)$ for $\text{LiAlO}_2(\text{s})$ from Eq. (31) and that of $\text{CaO}(\text{s})$, $\text{LiF}(\text{s})$, and $\text{CaF}_2(\text{s})$ from literature [17] and represented as

$$\Delta_{\text{f}} G_{\text{m}}^0(T) \text{ kJ mol}^{-1} (\pm 5.6) = -2341.2 + 0.4240 (T (\text{K})), \quad (734 \leq T (\text{K}) \leq 843). \quad (37)$$

3.3. Comparison of Gibbs energies of formation of $\text{LiAl}_5\text{O}_8(\text{s})$, $\text{LiAlO}_2(\text{s})$ and $\text{Li}_5\text{AlO}_4(\text{s})$ determined using KEQMS and solid-state galvanic cell

The values of standard molar Gibbs energies of formation of $\text{LiAl}_5\text{O}_8(\text{s})$, $\text{LiAlO}_2(\text{s})$ and $\text{Li}_5\text{AlO}_4(\text{s})$ determined from KEQMS and solid-state galvanic cell techniques are plotted as a function of temperature and shown in Fig. 6. The figure shows that values of

$\Delta_{\text{f}} G_{\text{m}}^0(T)$ are in close agreement and can be safely extrapolated to the entire temperature range. Thus, simultaneous use of KEQMS and solid-state galvanic cell study increases the experimental temperature range.

3.4. Measurement of heat capacities of ternary oxides of the system Li–Al–O

The isobaric molar heat capacities of $\text{LiAl}_5\text{O}_8(\text{s})$, $\text{LiAlO}_2(\text{s})$ and $\text{Li}_5\text{AlO}_4(\text{s})$ as a function of temperature were measured from (i) 127 to 308 and (ii) 308–868 K. The variation of heat capacities of these ternary oxides in per gram-atom were plotted as a function of temperature and shown in Fig. 7. The figure shows that heat capacity for $\text{LiAlO}_2(\text{s})$ in per gram-atom is more compared to other two ternary oxides and can be effectively used as blanket material for breeding in nuclear reactors. Kleykamp [8] has already reported the heat capacity data of $\text{LiAlO}_2(\text{s})$ from 298 to 1700 K. Heat capacity values of $\text{LiAlO}_2(\text{s})$ determined from DSC studies are in close agreement with that of literature [8]. However, literature on heat capacity values of $\text{LiAl}_5\text{O}_8(\text{s})$ and $\text{Li}_5\text{AlO}_4(\text{s})$ and low-temperature heat capacity values of ternary aluminates are not available. The individual values of heat capacities were fitted as a function of temperature in low and high-temperature ranges and are represented as

(a) 127–298 K

$$C_{\text{p,m}}^0(\text{LiAl}_5\text{O}_8) \text{ J K}^{-1} \text{ mol}^{-1} = -130.2 + 1.6994 (T (\text{K})) - 0.0018(T (\text{K}))^2 \quad (38)$$

$$C_{\text{p,m}}^0(\text{LiAlO}_2) \text{ J K}^{-1} \text{ mol}^{-1} = -45.2 + 0.6948 (T (\text{K})) - 0.0010(T (\text{K}))^2 \quad (39)$$

$$C_{\text{p,m}}^0(\text{LiAl}_5\text{O}_4) \text{ J K}^{-1} \text{ mol}^{-1} = -48.2 + 1.2035 (T (\text{K})) - 0.0016 (T (\text{K}))^2 \quad (40)$$

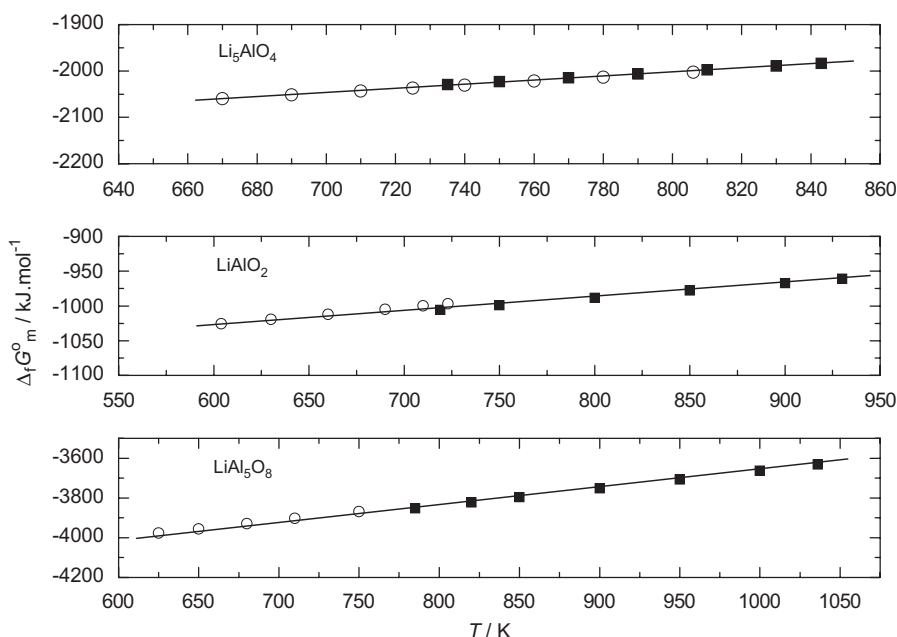


Fig. 6. Comparison of $\Delta_{\text{f}} G_{\text{m}}^0$ of ternary oxides determined from KEQMS and solid-state galvanic cell techniques: (O) KEQMS, (■) solid-state galvanic cell and solid line: combined fit of both the experimental data.

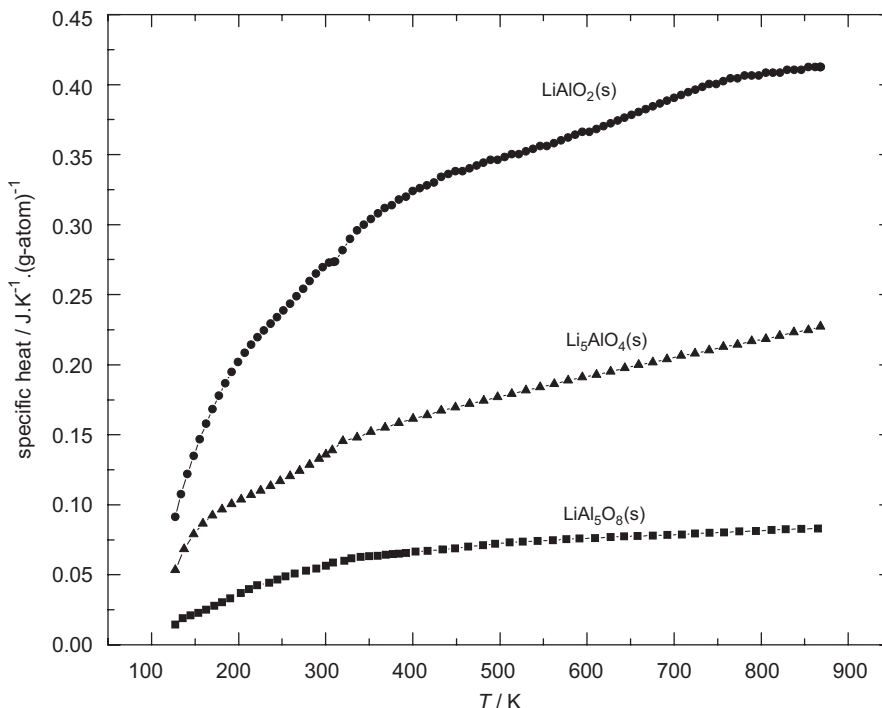


Fig. 7. Specific heat of ternary oxides in per gram-atom as a function of temperature.

Table 4
 $\Delta_f H_m^0(298.15 \text{ K})$ of lithium aluminates

Compound	$\Delta_f H_m^0(298.15 \text{ K}) \text{ kJ mol}^{-1}$			
	KEQMS (second law)	KEQMS (third law)	Galvanic cell (second law)	Literature
LiAl ₅ O ₈ (s)	−4517.2	−4487.8	−4535.9	−4577.5 [18]
LiAlO ₂ (s)	−1190.5	−1187.2	−1176.4	−1190.0 [17]
Li ₅ AlO ₄ (s)	−2360.2	−2417.1	−2360.1	−2391.9 [18]

(b) 308–868 K

$$C_{p,m}^o(\text{LiAl}_5\text{O}_8)\text{JK}^{-1}\text{mol}^{-1} = 258.3 + 0.0734(T(\text{K})) - 5749075.9(T(\text{K}))^{-2} \quad (41)$$

$$C_{p,m}^o(\text{LiAlO}_2)\text{JK}^{-1}\text{mol}^{-1} = 82.1 + 0.0344(T(\text{K})) - 184270.1(T(\text{K}))^{-2} \quad (42)$$

$$C_{p,m}^o(\text{Li}_5\text{AlO}_4)\text{JK}^{-1}\text{mol}^{-1} = 161.2 + 0.1462(T(\text{K})) - 2851348.0(T(\text{K}))^{-2} \quad (43)$$

3.5. Thermo-chemical stabilities of lithium aluminates

Guggi et al. [19] have discussed the thermal stability of these ternary aluminates and reported the heats of formation from the constituent oxides for one mole of Li₂O. Ikeda et al. [1] have determined the heats of formation of these oxides from the elements at 298.15 K, $\Delta_f H^0(298.15 \text{ K})$, using their high-temperature vaporization studies. In this study, same has been calculated using solid-state galvanic cell and Knudsen effusion mass spectrometric data. These values are in close agreement with

that of Guggi et al. [19] and Ikeda et al. [1] and tabulated in Table 4.

3.6. Construction of thermodynamic table for ternary oxides of Li–Al–O system

The Gibbs energies of formation of LiAl₅O₈(s), LiAlO₂(s) and Li₅AlO₄(s) obtained from KEQMS {Eqs. (11)–(13)} and galvanic cell techniques {Eqs. (25), (31) and (37)} were used for second law analysis to determine the standard molar enthalpy of formation, $\Delta_f H_m^0(298.15 \text{ K})$ and the standard molar entropies $S_m^0(298.15 \text{ K})$. Isobaric molar heat capacities from Eqs. (41)–(43) and standard molar Gibbs energies of formation for LiAl₅O₈(s), LiAlO₂(s) and Li₅AlO₄(s) from Eqs. (11)–(13) and (25), (31) and (37) were used as primary data for second law analysis and extrapolated to 1000 K as required. The partial pressure data obtained from KEMQS technique at each experimental temperature were treated by the third law method to derive the values of $\Delta_f H^0(298.15 \text{ K})$. It was observed that for LiAl₅O₈(s), LiAlO₂(s), the values of $\Delta_f H^0(298.15 \text{ K})$ obtained by second and third law treatment are in good agreement with that of literature [1,18]. However, for Li₅AlO₄(s), the values obtained by the third law method are more negative compared to second law value. For construction of thermodynamic tables for ternary oxides, average values of $\Delta_f H^0(298.15 \text{ K})$ obtained from second law analysis of this study and that of

Table 5
Thermodynamic functions for the compound $\text{LiAl}_5\text{O}_8(\text{s})$

T (K)	$^*C_p^0$ ($\text{J K}^{-1} \text{mol}^{-1}$)	H^0 (kJ mol^{-1})	G^0 (kJ mol^{-1})	S^0 ($\text{J K}^{-1} \text{mol}^{-1}$)	$H_T^0 - H_{298.15}^0$ (J mol^{-1})	fef ($\text{J K}^{-1} \text{mol}^{-1}$)	$\Delta_f H^0$ (kJ mol^{-1})	$\Delta_f G^0$ (kJ mol^{-1})
298.15	216.4	-4541.6	-4587.9	155.2	0	155.2	-4541.6	-4292.5
300	216.5	-4541.2	-4588.4	157.4	400	156.1	-4541.7	-4291.2
350	237.1	-4529.8	-4597.1	192.4	11,800	158.7	-4543.6	-4249.2
400	251.7	-4517.6	-4607.6	225.1	24,000	165.1	-4545.1	-4207.1
450	262.9	-4504.7	-4619.6	255.4	36,900	173.4	-4546.2	-4164.8
500	272.0	-4491.3	-4633.1	283.6	50,300	183.0	-4550.2	-4122.0
550	279.7	-4477.5	-4648.0	309.9	64,100	193.4	-4550.9	-4079.2
600	286.4	-4463.4	-4664.1	334.5	78,200	204.2	-4551.6	-4036.3
650	292.4	-4448.9	-4681.4	357.7	92,700	215.1	-4552.1	-3993.3
700	297.9	-4434.2	-4699.9	379.6	107,400	226.2	-4552.7	-3950.4
750	303.1	-4419.1	-4719.3	400.3	122,500	237.0	-4553.1	-3907.3
800	308.0	-4403.8	-4739.8	420.0	137,800	247.8	-4553.6	-3864.2
850	312.7	-4388.3	-4761.4	438.9	153,300	258.5	-4554.2	-3821.2
900	317.3	-4372.6	-4783.8	456.9	169,000	269.1	-4555.0	-3778.1
950	321.7	-4356.6	-4807.0	474.1	185,000	279.4	-4609.1	-3733.8
1000	325.9	-4340.4	-4831.1	490.7	201,200	289.5	-4609.2	-3687.8

* Estimated values of C_p .

Table 6
Thermodynamic functions for the compound $\text{Li}_5\text{AlO}_4(\text{s})$

T (K)	$^*C_p^0$ ($\text{J K}^{-1} \text{mol}^{-1}$)	H^0 (kJ mol^{-1})	G^0 (kJ mol^{-1})	S^0 ($\text{J K}^{-1} \text{mol}^{-1}$)	$H_T^0 - H_{298.15}^0$ (J mol^{-1})	fef ($\text{J K}^{-1} \text{mol}^{-1}$)	$\Delta_f H^0$ (kJ mol^{-1})	$\Delta_f G^0$ (kJ mol^{-1})
298.15	168.4	-2379.8	-2418.1	128.6	0	128.6	-2379.8	-2244.0
300	173.6	-2379.5	-2418.4	129.6	300	128.6	-2379.9	-2243.2
350	189.3	-2370.4	-2425.6	157.6	9400	130.7	-2381.3	-2220.3
400	202.1	-2360.6	-2434.1	183.8	19,200	135.8	-2382.4	-2197.2
450	213.1	-2350.2	-2443.9	208.2	29,600	142.4	-2383.5	-2174.0
500	223.1	-2339.3	-2454.9	231.2	40,500	150.2	-2399.6	-2149.1
550	232.4	-2327.9	-2467.0	252.9	51,900	158.5	-2400.2	-2124.0
600	241.2	-2316.1	-2480.2	273.5	63,700	167.3	-2400.4	-2098.9
650	249.7	-2303.8	-2494.3	293.1	76,000	176.2	-2400.1	-2073.8
700	257.9	-2291.1	-2509.4	311.9	88,700	185.2	-2399.4	-2048.7
750	265.9	-2278.0	-2525.5	330.0	101,800	194.3	-2398.4	-2023.7
800	273.9	-2264.5	-2542.4	347.4	115,300	203.3	-2397.1	-1998.7
850	281.7	-2250.6	-2560.3	364.3	129,200	212.3	-2395.4	-1973.9
900	289.5	-2236.3	-2578.8	380.6	143,500	221.3	-2393.4	-1949.1
950	297.1	-2221.7	-2598.3	396.4	158,100	230.0	-2401.8	-1924.3
1000	304.8	-2206.6	-2618.5	411.9	173,200	238.7	-2399.0	-1899.3

* Estimated values of C_p .

literature were used as primary data. Thermodynamic table includes the basic functions such as: $\Delta_f H^0(298.15 \text{ K})$, $S^0(298.15 \text{ K})$, $S^0(T)$, $C_p^0(T)$, $H^0(T)$, $\{H^0(T) - H^0(298.15 \text{ K})\}$, $G^0(T)$, $\Delta_f H^0(T)$, $\Delta_f G^0(T)$ and free energy function (fef) which were calculated using 'FACTSAGE thermo-chemical database' software [18]. The molar heat capacity values of $\text{Li}(\text{s})$, $\text{Al}(\text{s})$ and $\text{O}_2(\text{g})$ required for the second law analysis have been taken from the 'FACTSAGE thermo-chemical database' [18] and the thermodynamic values of the most stable phases were used. After calculation of all the thermodynamic functions, the values obtained at selected temperatures from 298 to 1000 K are tabulated and are given in Tables 5 and 6 for $\text{LiAl}_5\text{O}_8(\text{s})$ and $\text{Li}_5\text{AlO}_4(\text{s})$, respectively. Thermodynamic table for $\text{LiAlO}_2(\text{s})$ is already available in literature [18] hence it was not constructed in this study.

4. Conclusion

Standard molar Gibbs energies of formation of $\text{LiAl}_5\text{O}_8(\text{s})$, $\text{LiAlO}_2(\text{s})$ and $\text{Li}_5\text{AlO}_4(\text{s})$ evaluated from KEQMS and solid-state galvanic cell techniques. This study shows that RGA based on quadrupole mass spectrometer can effectively produce reliable thermodynamic data using Knudsen effusion mass spectrometric technique on proper calibration. However, the present system is

only suitable for partial pressure measurements of permanent gaseous species.

Acknowledgment

The authors gratefully acknowledge the help of Dr. K. Krishnan from Fuel Chemistry Division, BARC for X-ray diffraction analysis.

References

- [1] Y. Ikeda, H. Ito, G. Matsumoto, *J. Nucl. Mater.* 97 (1981) 47.
- [2] A. La Ginestra, M. Lo Jacono, P. Porta, *J. Thermal Anal.* 4 (1972) 5.
- [3] W. Heyi, Z. Jumke, L. Yangming, *J. Nucl. Mater.* 208 (1994) 195.
- [4] J.N. Singh, J.T. Dusek, J.W. Sim, *Ceram. Bull.* 60 (6) (1981) 629.
- [5] F.M. Gray, in: *Polymer Electrolyte*, R.C.S. Materials Monographs, The Royal Society of Chemistry, Cambridge, 1977.
- [6] F. Okaszomer, S. Naci Koc, I. Boz, M. Ali Gurkayank, *Mater. Res. Bull.* 39 (2004) 715.
- [7] R.A. Ribeiro, G.G. Silva, N.D.S. Mohallem, *J. Phys. Chem. Solids* 62 (2001) 857.
- [8] H. Kleykamp, *J. Nucl. Mater.* 270 (1999) 372.
- [9] G.A. Murray, R.A. Kematich, C.E. Myers, *High Temp. Sci.* 26 (1990) 4.
- [10] V.L. Stolyarova, D.U. Sichen, S. Seetharaman, *Vacuum* 46 (8–10) (1995) 871.
- [11] J.A. Basford, M.D. Boeckmann, R.E. Ellefson, A.R. Filippelli, D.H. Holkeboer, L. Lieszkovszky, C.M. Stupak, *J. Vac. Sci. Technol. A* 11 (3) (1993) A22.

- [12] M.C. Cowen, W. Allison, J.H. Batey, *J. Vac. Sci. Technol. A* 12 (1) (1994) 228.
- [13] M.G. Rao, C. Dong, *J. Vac. Sci. Technol. A* 15 (3) (1997) 1312.
- [14] J.B. Mann, *J. Chem. Phys.* 46 (1967) 1646.
- [15] J. Huang, T. Furukawa, K. Aoto, *J. Chem. Thermodyn.* 38 (2006) 1.
- [16] S.K. Rakshit, S.C. Parida, S. Dash, Z. Singh, B.K. Sen, V. Venugopal, *J. Solid State Chem.* 180 (2007) 523.
- [17] M.W. Chase Jr., JANAF thermochemical tables, 4th ed, *J. Phys. Chem. Ref. Data* 23 (1995) Monograph No. 9.
- [18] FactSage, version 5.3.1, Thermo-Chemical Database Software, Thermfact, GTT Technologies, Germany, 1976–2004.
- [19] D. Guggi, H.R. Ihle, A. Neubert, in: *Proceedings of the 9th Symposium on Fusion Technology*, Garmisch-Partenkirchen, Fed. Rep. Germany, Pergamon, Oxford, 1976.